**Cell Host & Microbe, Volume *32***

## Supplemental information

# Age-dependent heterogeneity in the antigenic effects of mutations to influenza hemagglutinin

**Frances C. Welsh, Rachel T. Eguia, Juhye M. Lee, Hugh K. Haddox, Jared Galloway, Nguyen Van Vinh Chau, Andrea N. Loes, John Huddleston, Timothy C. Yu, Mai Quynh Le, Nguyen T.D. Nhat, Nguyen Thi Le Thanh, Alexander L. Greninger, Helen Y. Chu, Janet A. Englund, Trevor Bedford, Frederick A. Matsen IV, Maciej F. Boni, and Jesse D. Bloom**

## Supplemental Figures

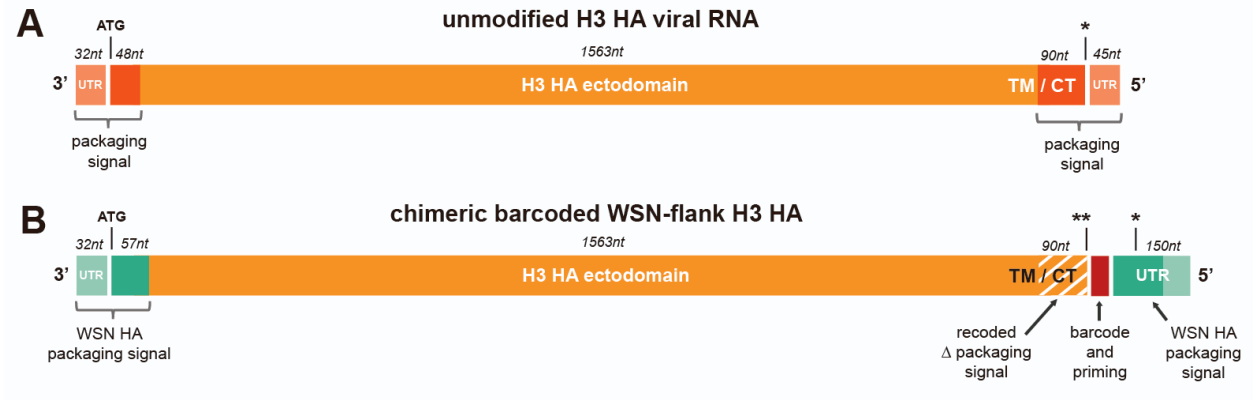


**Figure S1. Design of chimeric barcoded WSN-flank H3 HA construct, related to Figure 1.** All segments are shown in the reverse orientation of the negative-sense viral genome, with the 3' to 5' labels indicating ends in the negative-sense viral genome. Stop codons are denoted as asterisks. (A) Schematic of normal unmodified H3 HA. Influenza is multi-segmented, and proper packaging of vRNA into the virion relies on segment-specific RNA sequences called "packaging signals." These span both coding and noncoding regions at the 3' and 5' ends of the vRNA segment.[1] Packaging signals, untranslated regions (UTRs), ectodomain, transmembrane domain (TM), and cytoplasmic tail (CT) are labeled for a normal H3 HA. Corresponding nucleotide length is labeled based on sequence of A/Hong Kong/45/2019. (B) Schematic of chimeric WSN-flank H3 HA used for barcoding. To insert a barcode without disrupting vRNA packaging, we duplicate the full 5' packaging signal (including sequence from the coding region), and place it after the stop codons of the HA gene. The second stop codon was introduced to minimize polymerase read-through. We then insert a 16nt barcode and constant priming sequence after the stop codon and before the intact packaging signal. The native packaging sequence in the 5' coding region is synonymously recoded to avoid interference between duplicated sequences. Homology between the native and duplicated packaging signal could lead to barcode loss; we therefore included a stop codon in the duplicated packaging signal that will be in-frame if it replaces the native packaging signal. This ensures that loss of the barcode will generate a truncated, non-functional HA protein. The 3' and duplicated 5' packaging signals are taken from the lab-adapted A/WSN/1933 HA, as the library is grown using the other seven gene segments from this strain, and consistency between packaging signals helps achieve higher titers. See https://github.com/dms-vep/flu_h3_hk19_dms/tree/main/library_design/plasmid_maps for an annotated plasmid map of WSN-flank H3 HA.

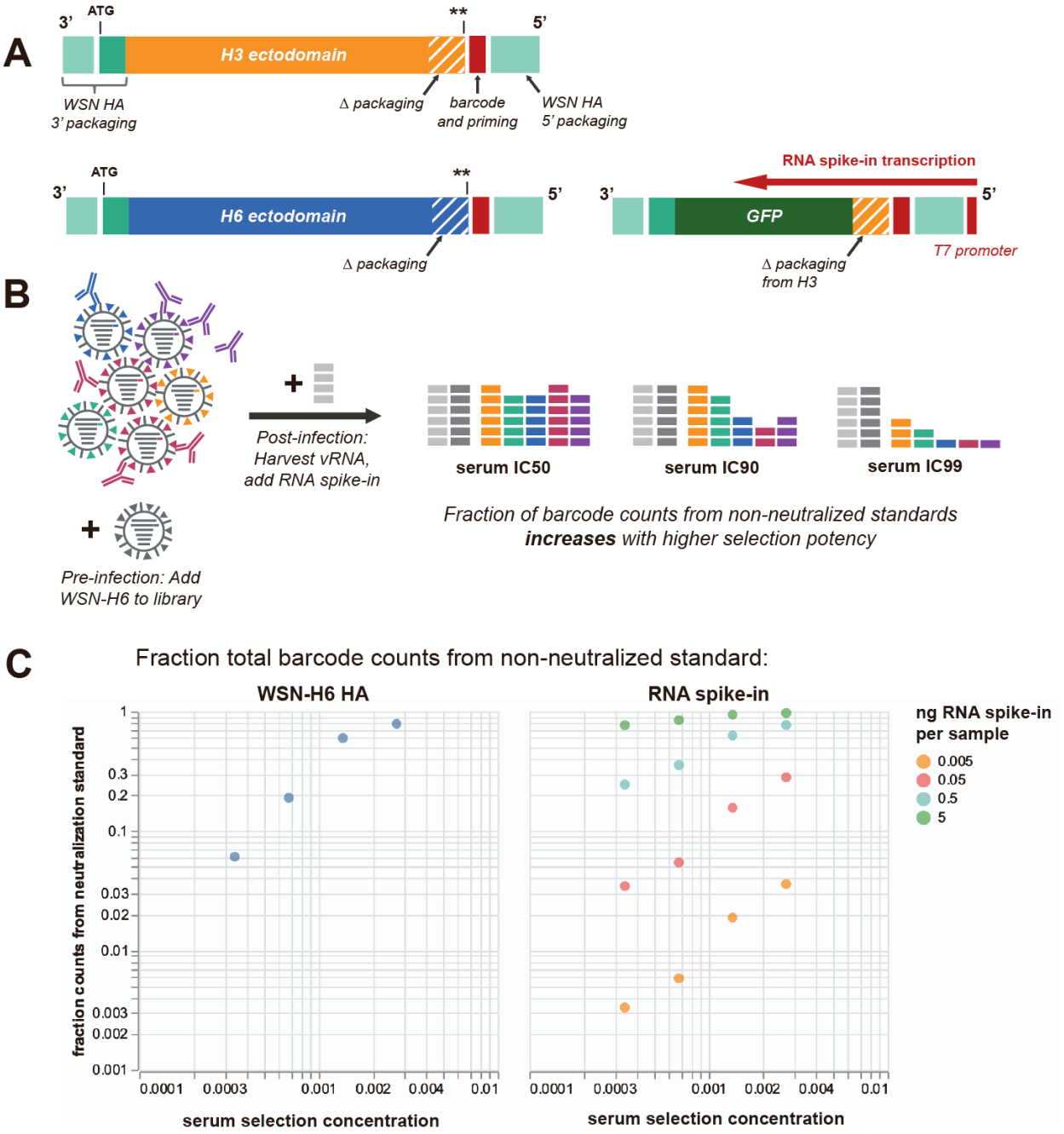


**Figure S2. Incorporation of non-neutralized standards to generate quantitative escape measurements, related to Figure 1.** (A) Design of WSN-H6 HA and RNA spike-in neutralization standards. The WSN-H6 HA standard is identical to the H3 HA library construct, but uses the ectodomain and 5' region from A/Turkey/Mass/1975, a low-pathogenicity avian HA strain (GenBank Accession AB296072.1).[2] The RNA spike-in is generated by *in vitro* transcription of a construct where the H3 HA ectodomain is replaced by GFP. See https://github.com/dms-vep/flu_h3_hk19_dms/tree/main/library_design/plasmid_maps for annotated plasmid maps of both standards. (B) WSN-H6 HA is spiked into the H3 HA library before incubating with serum and infecting cells. The RNA spike-in standard is added when

harvesting cellular RNA at 13 hours post-infection. As neither standard is neutralized by human sera, the number of barcodes from the standards remains constant, while H3 HA barcodes decrease at higher concentrations of neutralizing antibodies. The overall fraction of standard barcodes should therefore increase at a constant rate with increasing serum potency. (C) At a range of serum concentrations used for selections, the fraction of counts from the WSN-H6 HA neutralization standard increases in a consistent manner as the H3 HA variant library is more potently neutralized. Spiking in 0.05ng of RNA standard per sample achieves the same effect.

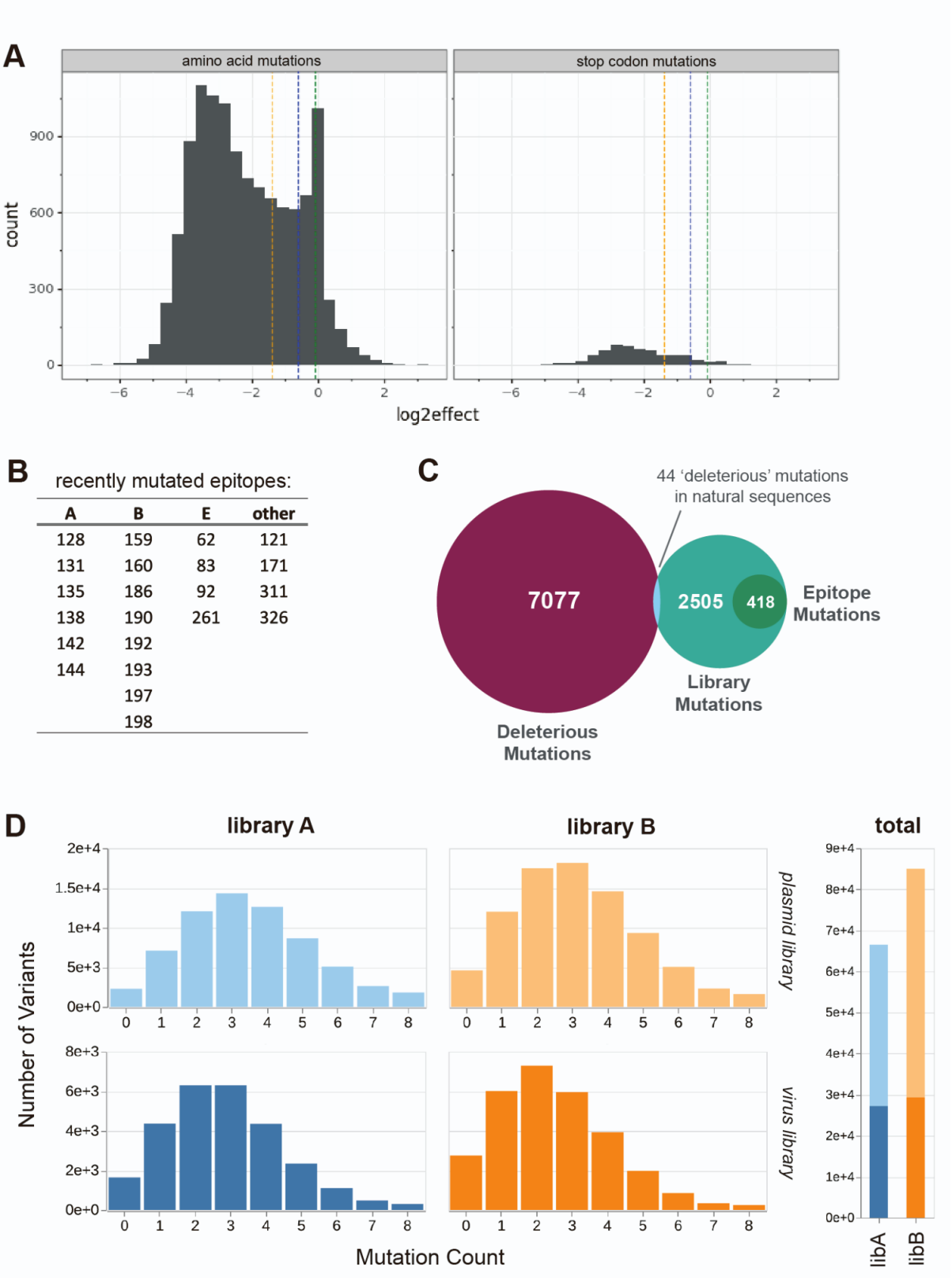


**Figure S3. Composition of H3 HA libraries, related to Figure 1.** (A) Functional effects of all single amino acid mutations to A/Perth/16/2009 H3 HA, calculated by Lee et al.[3] Vertical lines

delimit 75%, 90%, and 95% of the most deleterious stop codons. These quantiles are transposed onto all amino acid mutations, and 7,077 mutants corresponding to the 75th quantile of stop codons were excluded from the current library. (B) List of epitope sites, defined as sites that have been mutated in at least one major H3 HA clade between 2015 and 2021. These sites are randomly mutagenized in the library at a higher rate than the general non-deleterious mutations. (C) Visualization of types of mutations included in the library. In total, 7,077 mutations in the H3 HA ectodomain region were identified as functionally deleterious. 44 of these excluded mutants were identified in H3 HA strains circulating between 1968 and 2021, and added back into the library. This left 2,505 mutations to target in the library. 418 mutations at epitope sites were introduced at a higher frequency than general library mutations. (D) Distribution of mutations per variant in two fully independent plasmid libraries A and B, shown for both the starting plasmid libraries and the virus libraries after rescue and passaging. Variants were randomly mutagenized, targeting an average of 2-3 mutations per variant. The bar plot on the right shows the total number of variants in the plasmid library (approx. 65,000 and 85,000) and the virus library (approx. 30,000 in each library).

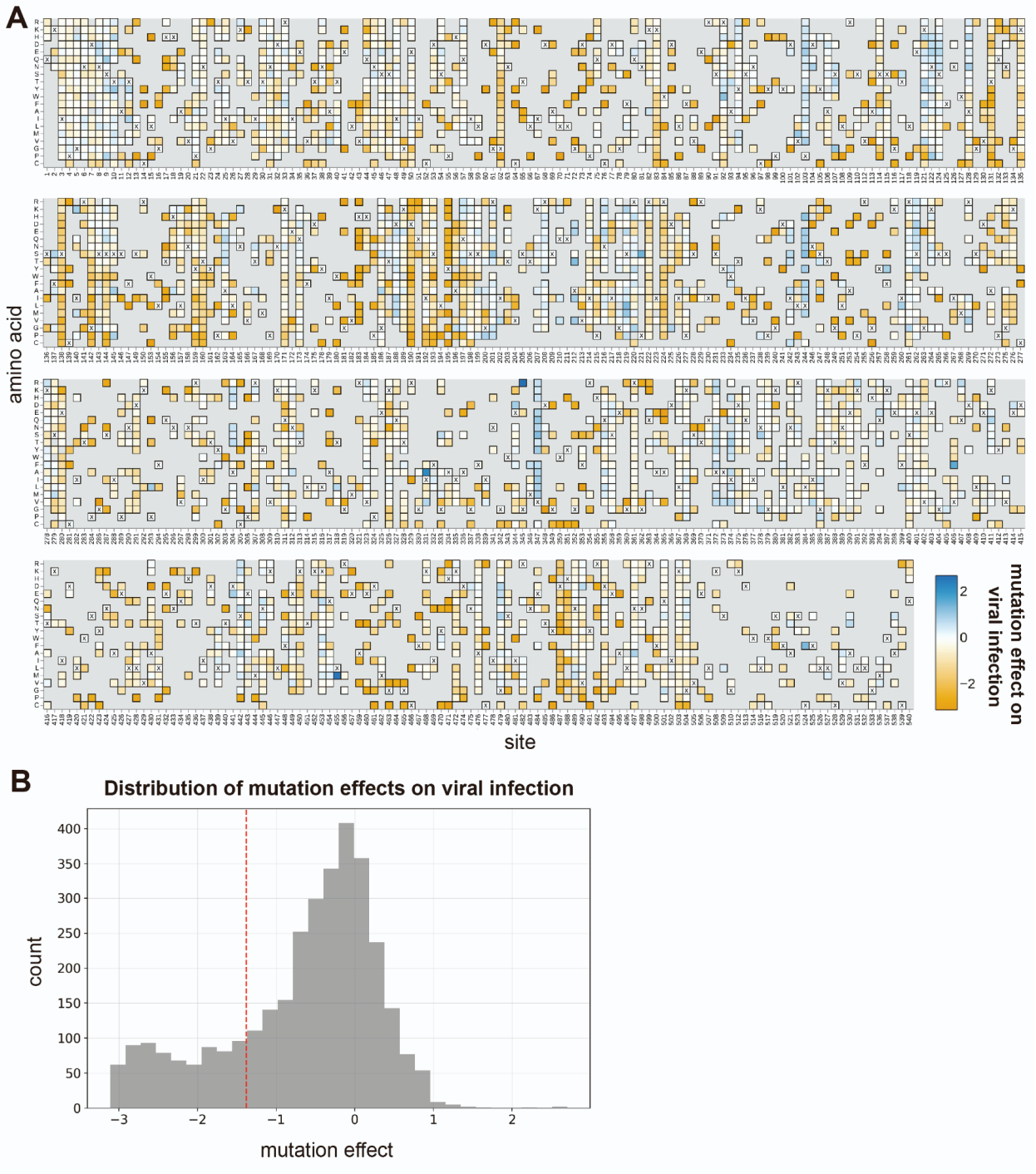


**Figure S4. Effects of H3 HA mutations on viral infection in cell culture, related to Figure 1.** (A) Heatmap showing the effects of mutations to A/Hong Kong/45/2019 H3 HA on viral infection in cell culture. Effects on viral infection were calculated by comparing the frequency of the mutation in the plasmid library to the final virus library, averaged between the independent libraries A and B. Lower values correspond to more deleterious effects. X indicates the wildtype amino acid in A/Hong Kong/45/2019 at each site, and light gray indicates mutations not sampled more than 3 times on average across both plasmid libraries. See https://dms-vep.org/flu_h3_hk19_dms/muteffects_observed_heatmap.html for full interactive,

zoomable heatmap. (B) Distribution of mutation effects on viral infection in cell culture. Dashed red line (mutation effect = -1.38) indicates the threshold used to exclude highly deleterious mutations from downstream analysis of serum neutralization effects.

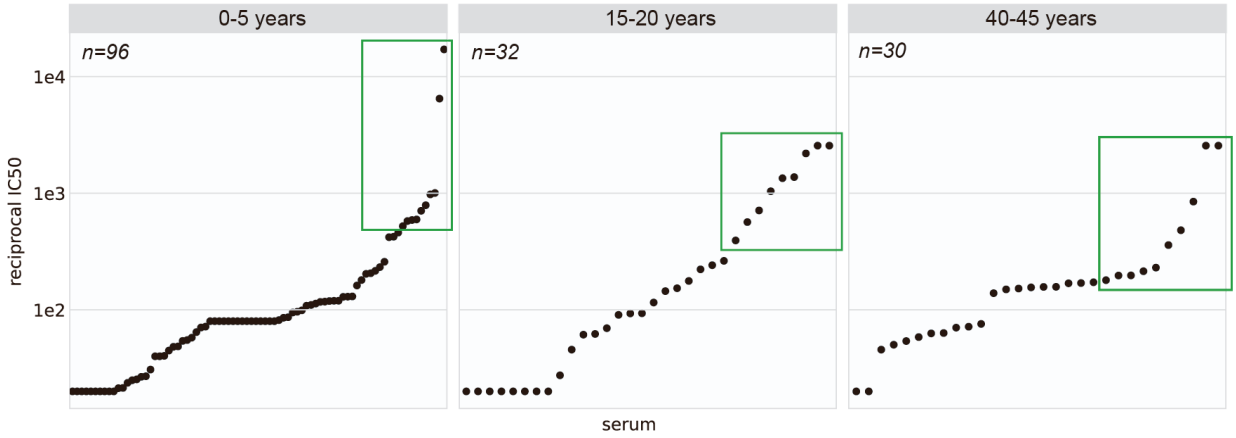


**Figure S5. Serum neutralizing titers against the A/Hong Kong/45/2019 HA barcoded library strain, related to Figure 2.** Neutralization assays were performed using influenza carrying GFP in the PB1 segment, as described previously;[4,5] see https://github.com/jbloomlab/flu_PB1flank-GFP_neut_assay for detailed protocol). Only a single replicate was run for each serum. IC50 values were calculated by fitting Hill-like curves using the neutcurve Python package (https://jbloomlab.github.io/neutcurve/). The ten sera from each age group with the highest neutralization activity against the parental library strain, boxed in green, were selected for serum escape mapping.

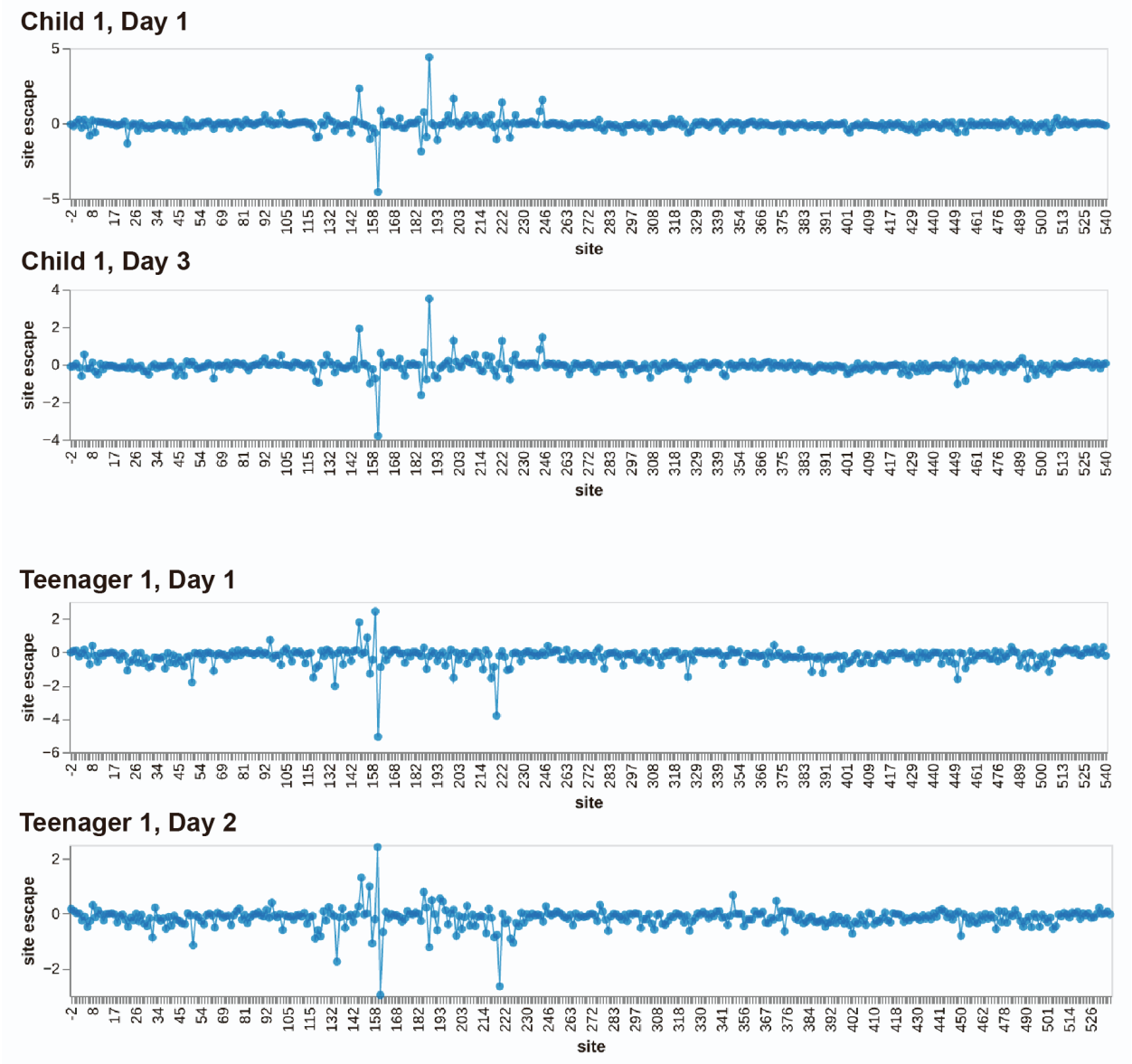


**Figure S6. Escape maps for sera collected on different days from the same individual, related to Figure 2.** One set of repeated samples comes from a child (sample 2388), and the other from a teenager (sample 3862). Line plots show summed escape scores of each sampled mutation at that site.

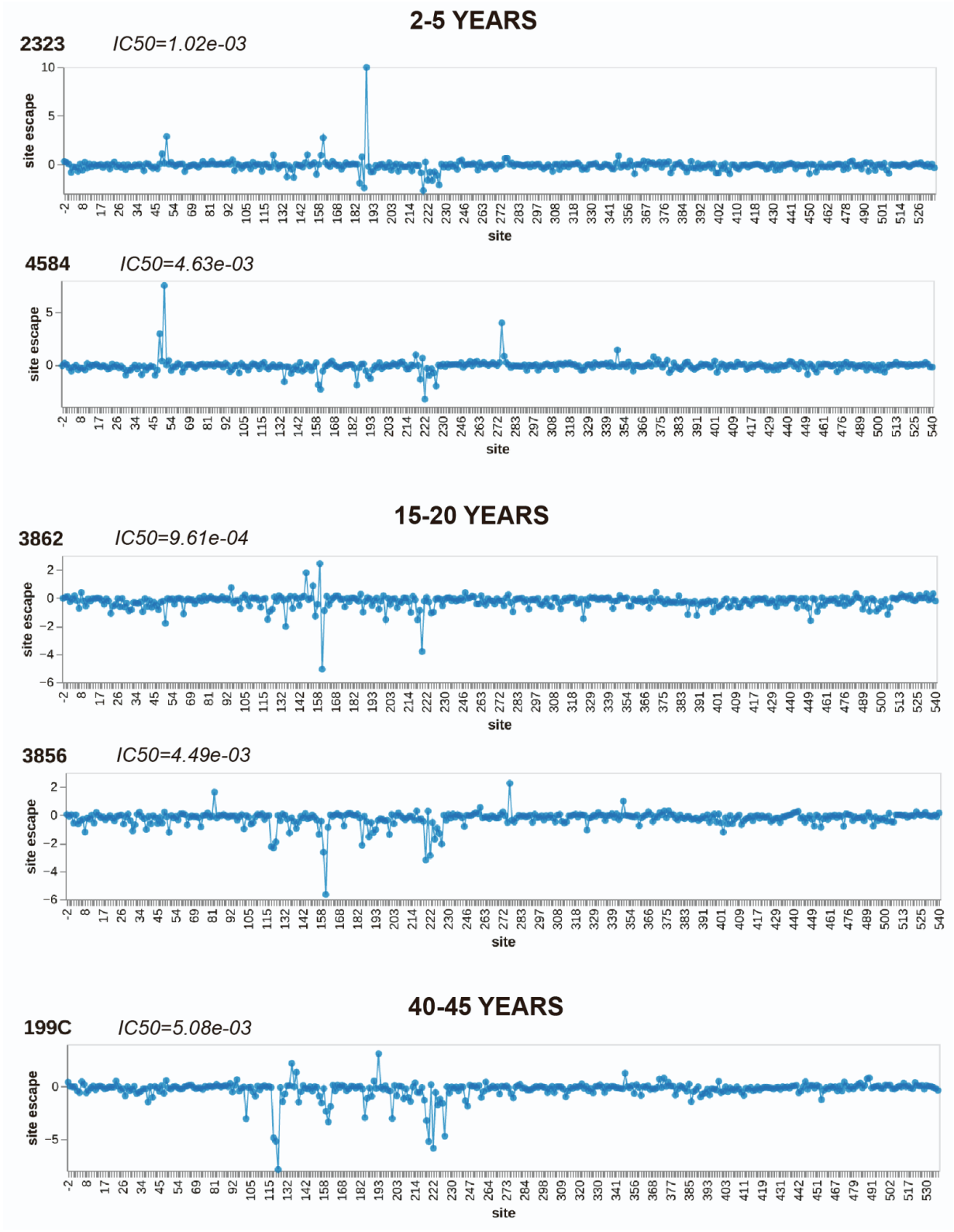


**Figure S7. Selected individual escape maps for sera in the 2020 cohort, analyzed against the A/Hong Kong/45/2019 library, related to Figure 2.** Line plots show summed escape scores of

each sampled mutation at that site. See https://github.com/dms-vep/flu_h3_hk19_dms/blob/main/figures/escape_map_lineplots/escape_maps_hk19.pdf for an extended version of this figure showing escape maps for all individuals in each age cohort, as well as the infant and elderly individual.

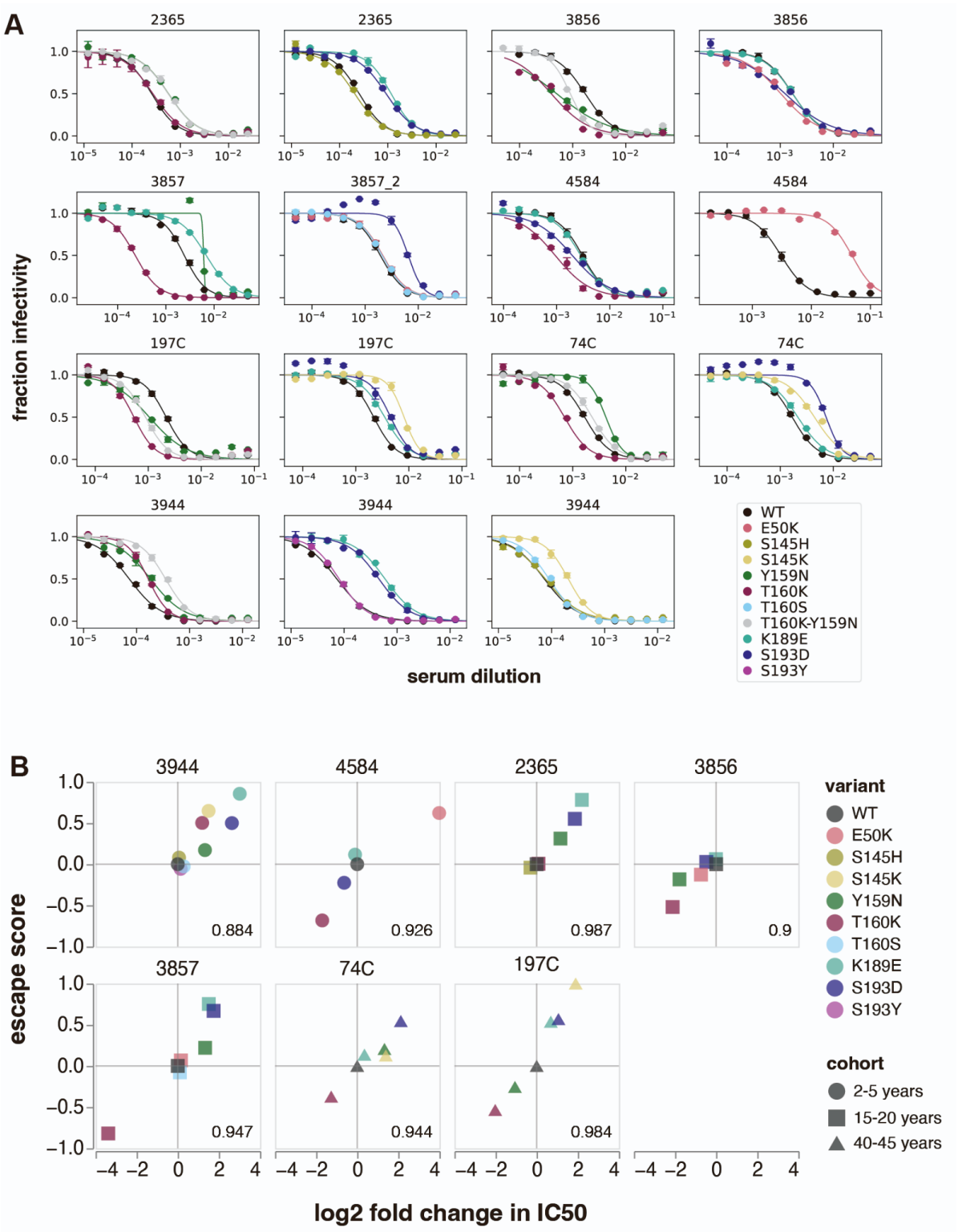


**Figure S8. Neutralization assay results for validation of deep mutational scanning measurements against the A/Hong Kong/45/2019 library, related to Figure 3.** (A) Neutralization curves for unmutated A/Hong Kong/45/2019 H3 HA ('WT') and selected mutants against seven

representative sera from different age cohorts. (B) Correlation between escape score and the log2 fold change in serum IC50 for each variant, plotted for each serum independently. Pearson R correlation is noted on each plot. The IC50 for each variant was compared to the IC50 for the wildtype strain run in the same experiment, to control for potential variation in serum concentration and cell number between independent experiments.

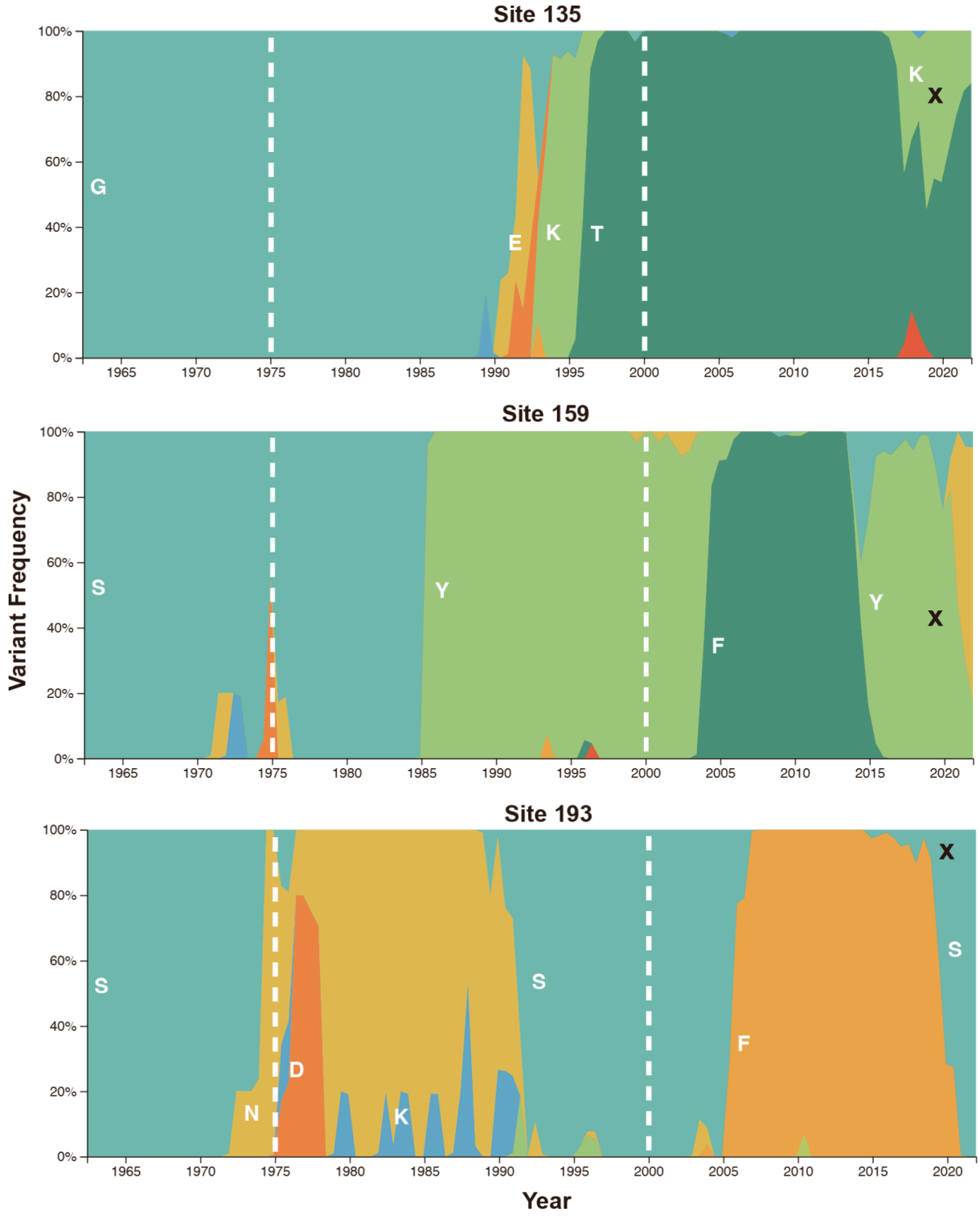


**Figure S9. Global frequency of variants at sites 135, 159, and 193, related to Figure 2.** Dashed lines indicate the earliest birthdate of individuals in the adult cohort (1975) and teenage cohort (2000). Black 'X' indicates the amino acid identity of the wildtype library strain, A/Hong Kong/45/2019. Frequency plot adapted from the Nextstrain real-time pathogen evolution website.[6,7]

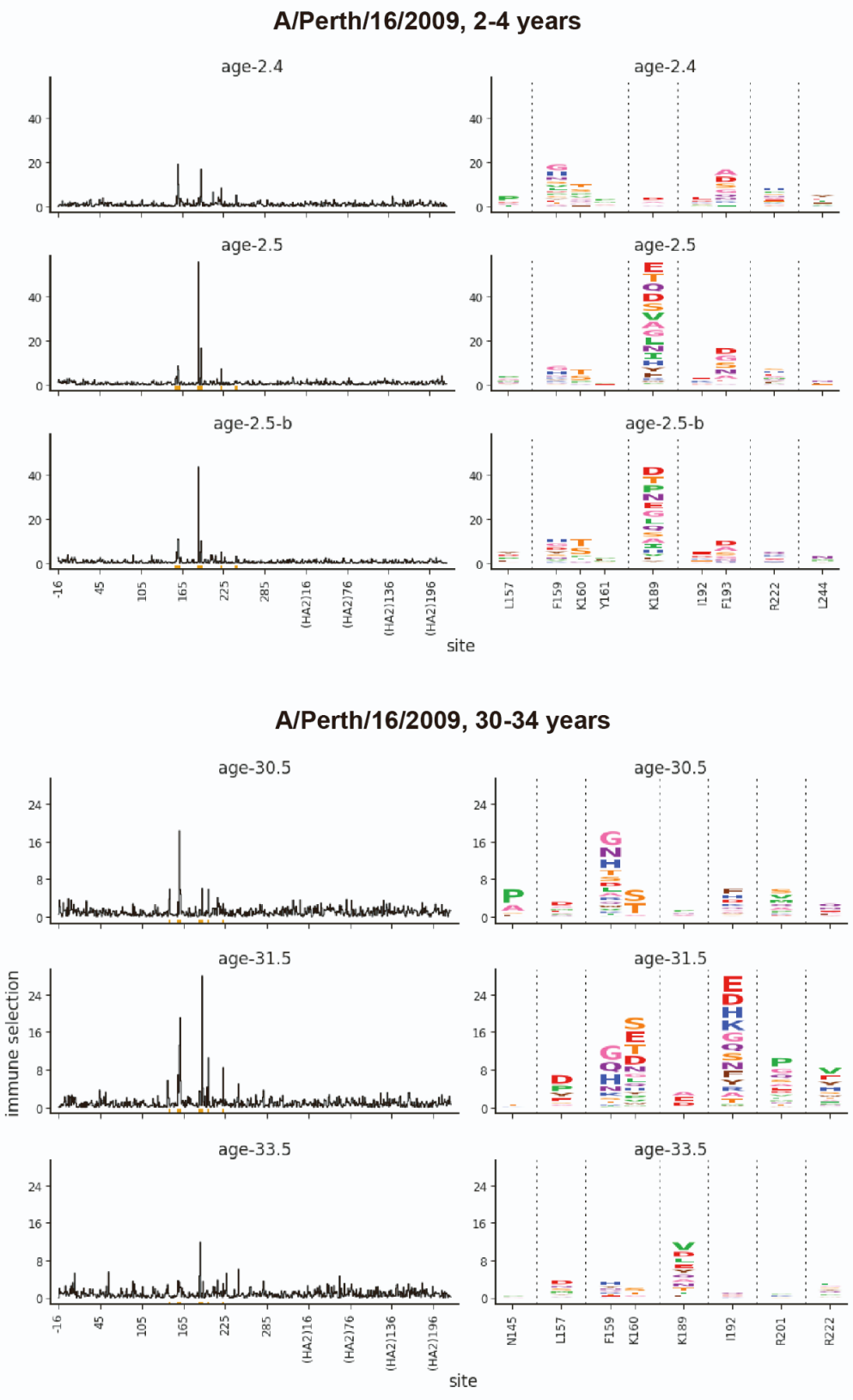


**Figure S10. Selected individual escape maps for each serum in the 2010-2011 cohort, analyzed against the A/Perth/16/2009 library, related to Figure 4.** Line plots show summed

escape scores of each sampled mutation at that site. Logo plots show mutation-level escape at key sites, where the height of each letter corresponds to the escape score for that amino acid substitution. Escape scores for singly-infected ferrets shown in **Figure 4** are data from the postinfection ferret samples originally published in Figure 6 of Lee et al. (2019).[8] See https://github.com/dms-vep/flu_h3_hk19_dms/blob/main/figures/escape_map_lineplots/escape_maps_perth09.pdf for an extended version of this figure showing escape maps for all individuals in each age cohort.

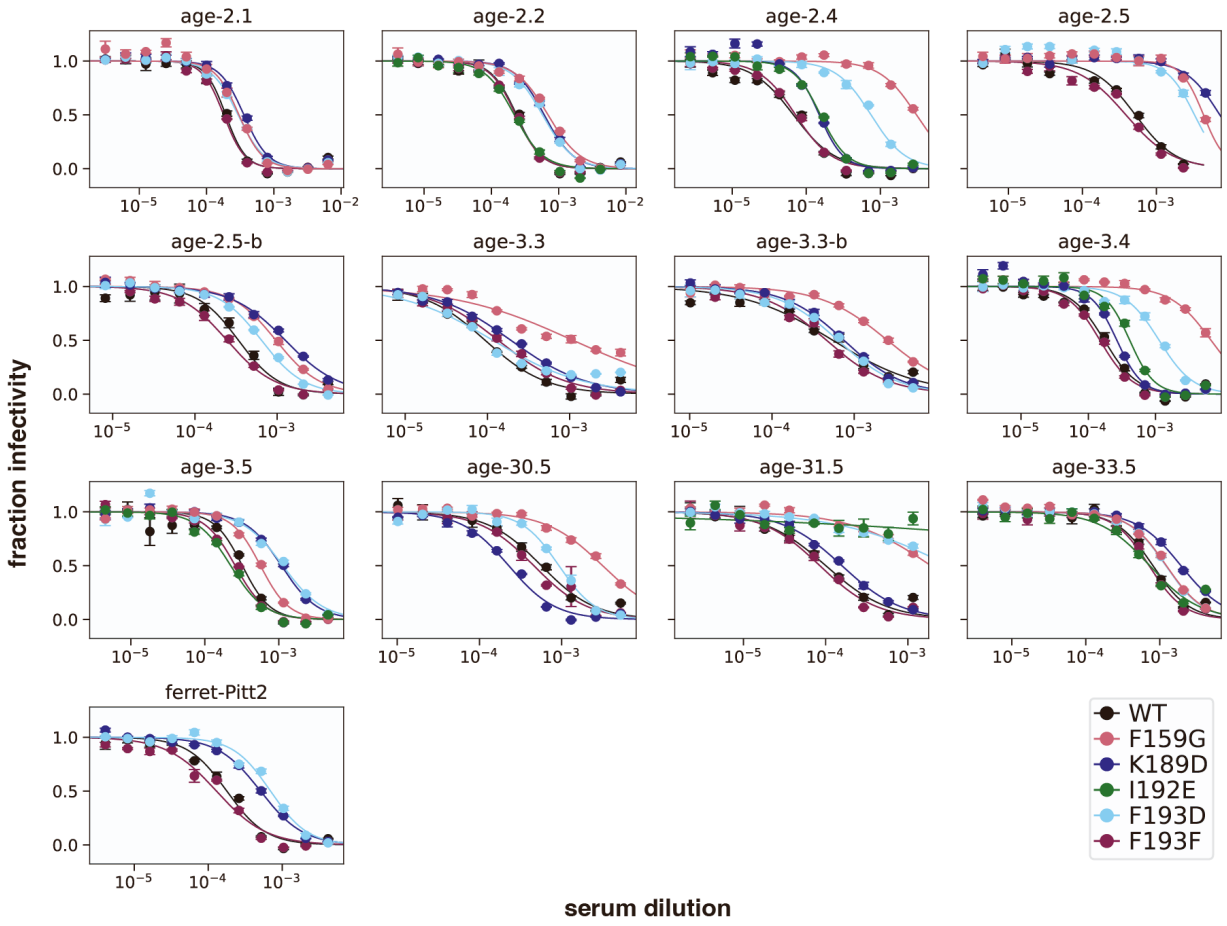


**Figure S11. Neutralization assay results for validation of deep mutational scanning measurements against the A/Perth/16/2009 library, related to Figure 4.** Neutralization curves are shown for unmutated A/Perth/16/2009 H3 HA ('WT') and selected mutants against all human sera from the 2010-2011 cohort, plus one representative ferret serum.

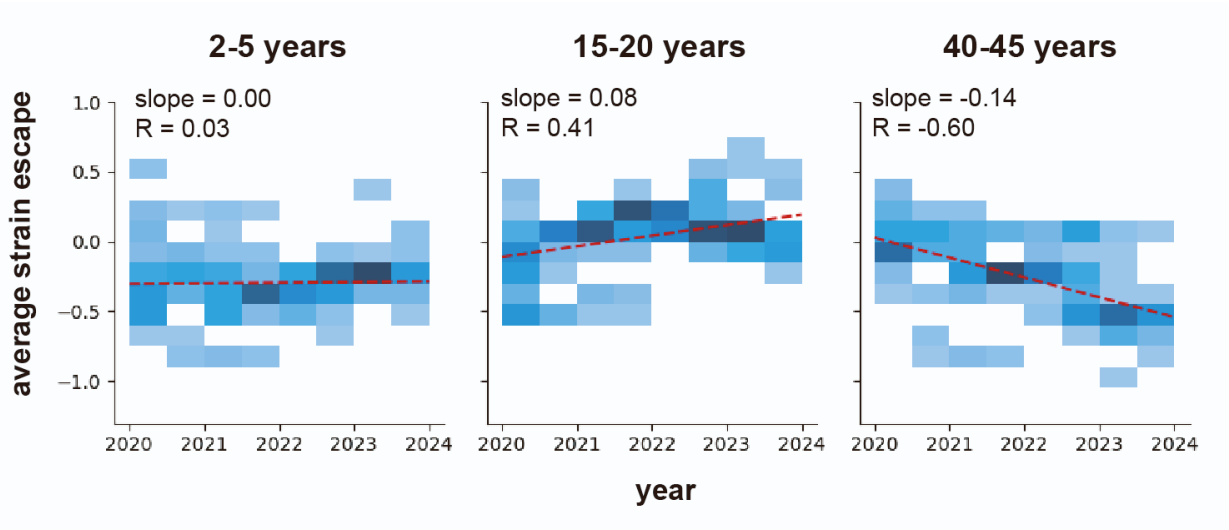


**Figure S12. Correlation between escape mapped in deep mutational scanning and actual H3N2 HA evolution after 2020, related to Figure 6.** This figure differs from Fig. 6B in that it only shows data for 240 H3N2 influenza strains circulating *after* serum collection, from 2020 to 2023. The slope is significantly lower for the adult cohort compared to the teenage ($p$=0.002) and child ($p$=0.045) cohorts. The difference between the teenage and child cohorts is not statistically significant ($p$=0.226).

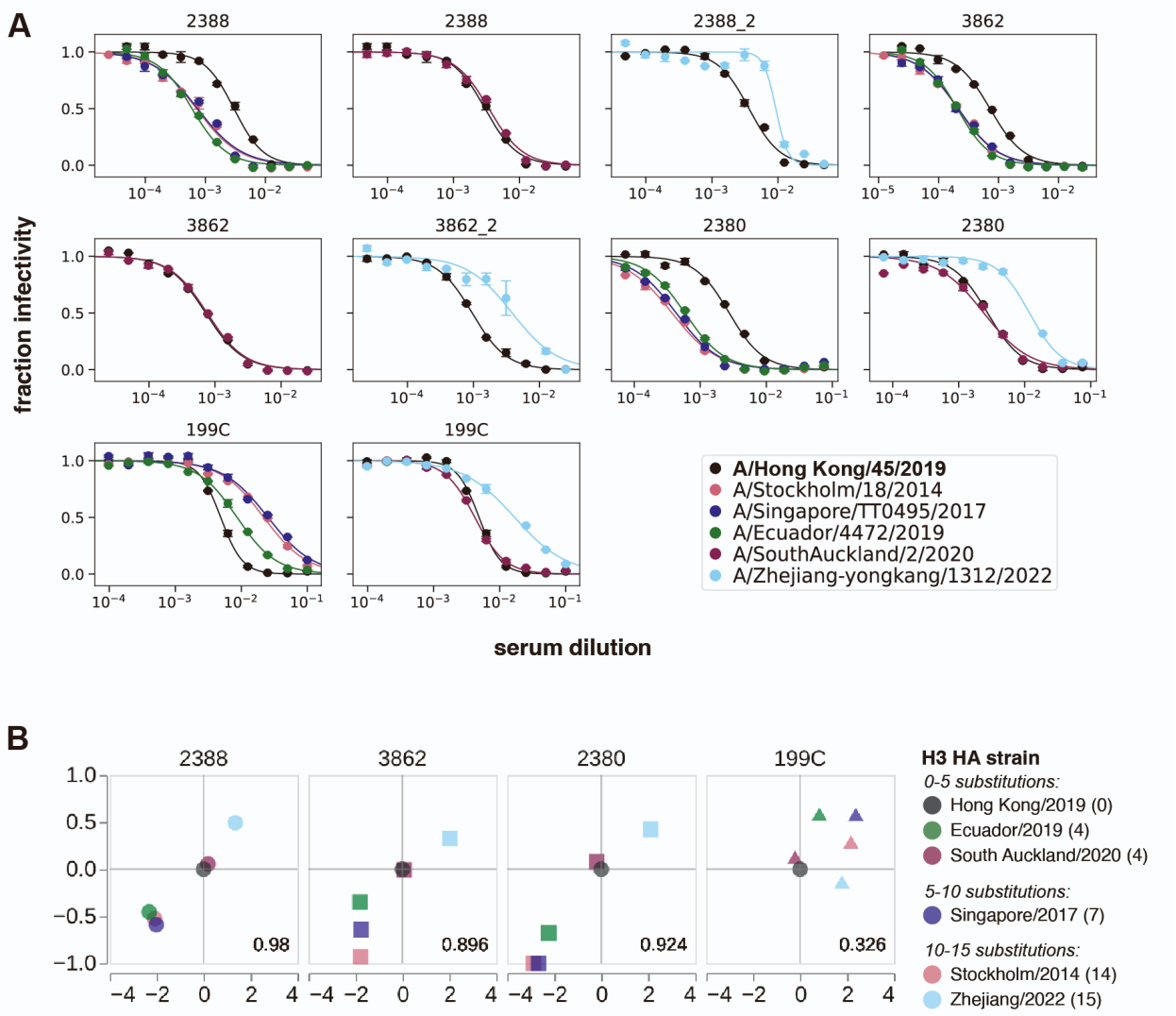


**Figure S13. Neutralization assay results for validation of predicted strain escape from deep mutational scanning measurements, related to Figure 6.** This figure shows the underlying data aggregated in Fig. 6C. (A) Neutralization curves for unmutated A/Hong Kong/45/2019 H3 HA and selected strains circulating from 2014 to 2022 against four representative sera from different age cohorts. 2388 - child; 3862 and 2380 - teenagers; and 199C - adult. (B) Correlation between escape score and the log2 fold change in serum IC50 for each strain, plotted for each serum independently. The number of substitutions relative to A/Hong Kong/45/2019 is noted in parentheses after the strain name. Pearson R correlation is noted on each plot. The IC50 for each variant was compared to the IC50 for the wildtype strain run in the same experiment, to control for potential variation in serum concentration and cell number between independent experiments.

| Study ID | Age at serum collection (in years) | Serum collection date (quarter) | Flu shot 1 date (quarter) | Flu shot 2 date (quarter) | Flu shot 3 date (quarter) | Immunocompromised | Recent intravenous IgG treatment? | Infection history |
|---|---|---|---|---|---|---|---|---|
| 2462 | 0.2 | Apr-June 2020 | None | None | None | No | No | unknown |
| 2323 | 3 | Apr-June 2020 | Oct-Dec 2019 | Oct-Dec 2018 | Oct-Dec 2017 | No | No | unknown |
| 2367 | 3 | Apr-June 2020 | Jul-Sep 2019 | Oct-Dec 2018 | Jan-Mar 2018 | No | No | unknown |
| 2388 | 4 | Apr-June 2020 | Oct-Dec 2019 | Oct-Dec 2017 | Jan-Mar 2017 | No | No | unknown |
| 2389 | 4 | Apr-June 2020 | Oct-Dec 2019 | Oct-Dec 2018 | Jul-Sep 2017 | No | No | unknown |
| 3944 | 4 | Apr-June 2020 | Oct-Dec 2019 | Oct-Dec 2017 | Jan-Feb 2017 | No | No | unknown |
| 3973 | 2 | Apr-June 2020 | Oct-Dec 2019 | Jan-Mar 2019 | Oct-Dec 2018 | Yes | No | unknown |
| 4584 | 2 | Apr-June 2020 | Oct-Dec 2019 | Jan-Mar 2019 | Jan-Mar 2018 | No | No | unknown |
| 4299 | 4 | Apr-June 2020 | Oct-Dec 2019 | Oct-Dec 2018 | Oct-Dec 2017 | Yes | No | unknown |
| 3862 | 15 | Apr-June 2020 | None | None | None | No | No | unknown |
| 2350 | 20 | Apr-June 2020 | Oct-Dec 2019 | unknown | unknown | Yes | No | unknown |
| 2365 | 17 | Apr-June 2020 | Oct-Dec 2018 | Oct-Dec 2016 | Jul-Sep 2013 | No | No | unknown |
| 2380 | 15 | Apr-June 2020 | Oct-Dec 2019 | Oct-Dec 2018 | Oct-Dec 2017 | No | No | unknown |
| 2382 | 19 | Apr-June 2020 | Jul-Sep 2018 | Oct-Dec 2017 | Jul-Sep 2015 | No | No | unknown |
| 3856 | 20 | Apr-June 2020 | Oct-Dec 2019 | Oct-Dec 2012 | None | Yes | No | Influenza B positive in Jan-Mar 2020 |
| 3857 | >15 years | Apr-June 2020 | unknown | unknown | unknown | unknown | No | unknown |
| 3866 | 18 | Apr-June 2020 | Oct-Dec 2018 | Oct-Dec 2017 | Oct-Dec 2016 | Yes | Yes | unknown |

**Table S1, related to Figure 2.** Age, serum collection date, recent vaccination history, and relevant medical history for the unvaccinated infant and individuals in the 2-5 and 15-20 year age cohorts from Seattle, Washington.

| Study ID | Birth year (approx) | Age at serum collection (in years) | Serum collection date (quarter) | Received flu vaccine in 2019-2020 season? | 2019-2020 flu vaccine date (quarter) | Received flu vaccine in 2018-2019 season? |
|---|---|---|---|---|---|---|
| 34C | 1975 | 45 | Apr-June 2020 | Yes | Oct-Dec 2019 | Yes |
| 199C | 1976 | 44 | Apr-June 2020 | Yes | Oct-Dec 2019 | Yes |
| 197C | 1978 | 42 | Jul-Sep 2020 | No | N/A | Yes |
| 18C | 1977 | 43 | Jul-Sep 2020 | Yes | Jul-Sep 2019 | Yes |
| 33C | 1977 | 43 | Jul-Sep 2020 | Yes | Oct-Dec 2019 | Yes |
| 215C | 1977 | 43 | Jul-Sep 2020 | Yes | Oct-Dec 2019 | Yes |
| 74C | 1978 | 42 | Oct-Dec 2020 | No | N/A | No |
| 210C | 1975 | 45 | Oct-Dec 2020 | Yes | Oct-Dec 2019 | Yes |
| 150C | 1977 | 43 | Oct-Dec 2020 | Yes | Oct-Dec 2019 | Yes |
| 68C | 1976 | 44 | Oct-Dec 2020 | No | N/A | Yes |

**Table S2, related to Figure 2.** Age, approximate birth year, serum collection date, and recent vaccination history for individuals in the 40-45 year age cohort from Seattle, Washington.

**Table S3.**

| Primers for amplifying WSN-flanked H3 HA coding sequence | |
|---|---|
| Forward linearizing primer (primer_088) | gcaaaactactggtcctgttatatgcatttgtagc |
| Reverse linearizing primer (primer_089) | ctcattatatacagatgttgcatcggatgttgcc |
| Primers for mutagenizing H3 HA ectodomain | |
| General mutagenic primer pool (forward and reverse) | https://github.com/dms-vep/flu_h3_hk19_dms/blob/main/library_design/hk19_primers.csv |
| Epitope primer pool (forward and reverse) | https://github.com/dms-vep/flu_h3_hk19_dms/blob/main/library_design/hk19_single_epitope_primers.csv |
| Paired epitope primer pool (forward and reverse) | https://github.com/dms-vep/flu_h3_hk19_dms/blob/main/library_design/hk19_paired_epitope_primers.csv |
| Primers for barcoding WSN-flanked H3 HA sequences | |
| Forward linearizing primer (primer_088) | gcaaaactactggtcctgttatatgcatttgtagc |
| Reverse barcoding primer (primer_090) | acactctttccctacacgacgctcttccgatctNNNNNNNNNNNNNNNNctcattatatacagatgttgc |
| Primers for amplifying H3 HA C-terminus with GFP overlap | |
| Forward GFP overlap primer (primer_115) | TGGACGAGCTGTACAAGTAATAGgttgagctgaagtcaggatacaaagattggatc |
| Reverse linearizing primer (primer_089) | ctcattatatacagatgttgcatcggatgttgcc |
| Primers for generating RNA spike-in template with T7 promoter | |
| Forward U12-annealing primer (primer_113) | agcaaaagcaggggaaaataaaaacaacc |
| Reverse T7-appending primer (primer_116) | TTACGATAATACGACTCACTATAGGGagtagaaacaagggtgtttttccttatatttctg |
| Primers for reverse transcription of viral barcodes | |
| Viral mRNA-annealing RT primer (primer_110) | ggcaacatccgatgcaacatctgtatataatga |
| Round one Illumina barcode sequencing preparation primers | |
| Illumina round 1 forward primer (primer_098) | GTGACTGGAGTTCAGACGTGTGCTCTTCCGATCTggcaacatccgatgcaacatctgtatataatgag |
| Illumina round 1 reverse primer (primer_099) | acactctttccctacacgacgctcttccgatct |

| Round two Illumina barcode sequencing preparation primers | |
|---|---|
| Unique i5 indexing prime | AATGATACGGCGACCACCGAGATCTACACxxxxxxxxxACACTCTTTCCCTACACGACGCTCTTCCGATCT<br><br>Where "xxxxxxxxxx" are NextFlex indices unique to each primer. |
| Unique i7 indexing primer | CAAGCAGAAGACGGCATACGAGATtatcttcagcGTGACTGGAGTTCAGACGTGTGCTCTTCCGATCT<br><br>Where "xxxxxxxxxx" are NextFlex indices unique to each primer. |

**Table S3, related to Figure 1.** Primers and sequences used for generating DNA constructs, mutagenizing the HA ectodomain, and amplifying and sequencing the barcode region, as referenced in methods.

## References


1. Li, X., Gu, M., Zheng, Q., Gao, R., and Liu, X. (2021). Packaging signal of influenza A virus. Virol. J. *18*, 36.

2. Sandbulte, M.R., Gao, J., Straight, T.M., and Eichelberger, M.C. (2009). A miniaturized assay for influenza neuraminidase-inhibiting antibodies utilizing reverse genetics-derived antigens. Influenza Other Respi. Viruses *3*, 233–240.

3. Lee, J.M., Huddleston, J., Doud, M.B., Hooper, K.A., Wu, N.C., Bedford, T., and Bloom, J.D. (2018). Deep mutational scanning of hemagglutinin helps predict evolutionary fates of human H3N2 influenza variants. Proc. Natl. Acad. Sci. U. S. A. *115*, E8276–E8285.

4. Hooper, K.A., and Bloom, J.D. (2013). A mutant influenza virus that uses an N1 neuraminidase as the receptor-binding protein. J. Virol. *87*, 12531–12540.

5. Doud, M.B., Lee, J.M., and Bloom, J.D. (2018). How single mutations affect viral escape from broad and narrow antibodies to H1 influenza hemagglutinin. Nat. Commun. *9*, 1386.

6. Hadfield, J., Megill, C., Bell, S.M., Huddleston, J., Potter, B., Callender, C., Sagulenko, P., Bedford, T., and Neher, R.A. (2018). Nextstrain: real-time tracking of pathogen evolution. Bioinformatics *34*, 4121–4123.

7. Neher, R.A., and Bedford, T. (2015). nextflu: real-time tracking of seasonal influenza virus evolution in humans. Bioinformatics *31*, 3546–3548.

8. Lee, J.M., Eguia, R., Zost, S.J., Choudhary, S., Wilson, P.C., Bedford, T., Stevens-Ayers, T., Boeckh, M., Hurt, A.C., Lakdawala, S.S., et al. (2019). Mapping person-to-person variation in viral mutations that escape polyclonal serum targeting influenza hemagglutinin. Elife *8*. 10.7554/eLife.49324.